Key Points:
- Ground-level TETRA-II events occur near maxima in lightning rates, hail, echo top heights, and vertically integrated liquid density
- Events occur in both high and low lightning frequency storms and close to maximum updraft development
- Events occur in association with multi-cell and squall line thunderstorms, but not single-cell storms

Supporting Information:
Supporting Information may be found in the online version of this article.

Correspondence to:
D. Smith,
dsmi229@lsu.edu

Thunderstorms Producing Sferic-Geolocated Gamma-Ray Flashes Detected by TETRA-II

Deirdre Smith[1] [iD], **Jill Trepanier[1]** [iD], **Samer T. Alnussirat[2]** [iD], **Michael L. Cherry[2]**, **Marc D. Legault[3]**, and **Donald J. Pleshinger[4]**

[1]Department of Geography & Anthropology, Louisiana State University, Baton Rouge, LA, USA, [2]Department of Physics & Astronomy, Louisiana State University, Baton Rouge, LA, USA, [3]Department of Physics, University of Puerto Rico at Bayamón, Bayamón, PR, USA, [4]Department of Pharmacology, Center for Lung Biology, University of South Alabama, Mobile, AL, USA

Abstract The terrestrial gamma-ray flash (TGF) and Energetic Thunderstorm Rooftop Array (TETRA-II) detected 22 X-ray/gamma-ray flash events associated with lightning between October 2015 and March 2019 across three ground-based detector locations in subtropical and tropical climates in Louisiana, Puerto Rico, and Panama. Each detector array consists of a set of bismuth germanate scintillators that record X-ray and gamma-ray bursts over the energy range 50 keV–6 MeV (million electron volts). TETRA-II events have characteristics similar to both X-ray bursts associated with lightning leaders and TGFs: sub-millisecond duration, photons up to MeV energies, and association with nearby lightning (typically within 3 km). About 20 of the 22 events are geolocated to individual lightning strokes via spatiotemporally coincident sferics. An examination of radar reflectivity and derived products related to events located within the Next Generation Weather Radar (NEXRAD) monitoring region indicates that events occur within mature cells of severe and non-severe multicellular and squall line thunderstorms, with core echo tops which are at or nearing peak altitude. Events occur in both high lightning frequency thunderstorm cells and low lightning frequency cells. Events associated with high frequency cells occur within 5 min of significant lightning jumps. Among NEXRAD-monitored events, hail is present within 8 km and 5 min of all except a single low-altitude cold weather thunderstorm. An association is seen with maximum thunderstorm development, lightning jumps, and hail cells, indicating that the TETRA-II X-ray/gamma-ray events are associated with the peak storm electrification and development of electric fields necessary for the acceleration of electrons to high energies.

1. Introduction

Microsecond-to-millisecond scale bursts of high energy radiation have been detected associated with thunderstorms and lightning from ground level, from aircraft and balloons, and from space. From space, terrestrial gamma-ray flashes (TGFs) were discovered in 1994 by the Burst and Transient Source Experiment (BATSE) aboard the Compton Gamma-ray Observatory (Fishman et al., 1994) and have since been observed at energies up to 40 million electron volts (MeV; Briggs et al., 2010; Dwyer & Smith, 2005; Grefenstette et al., 2009; Marisaldi et al., 2010). The connection with thunderstorms was recognized almost immediately, and TGFs have since been associated with individual lightning strokes via very low frequency or radio atmospheric (sferic) observations (Lu et al., 2010; Shao et al., 2010; Stanley et al., 2006; Williams et al., 2006). TGFs have been observed in space by the Reuven Ramaty High Energy Solar Spectroscopic Imager (RHESSI; Grefenstette et al., 2009), Fermi Gamma-ray Burst Monitor (GBM; Roberts et al., 2018), Astrorivelatore Gamma ad Immagini Leggero (AGILE; Marisaldi et al., 2015), BeppoSAX (Ursi et al., 2017), the Relativistic ELECtrons experiment (Panasyuk et al., 2016), and Atmosphere-Space Interaction Monitor (ASIM; Østgaard et al., 2019). From the ground, events have been reported mainly in association with lightning leaders (Abbasi et al., 2017; Chilingarian et al., 2010; Dwyer et al., 2004, 2005; Mallick et al., 2012; Moore et al., 2001; Pleshinger et al., 2019; Ringuette et al., 2013; Tran et al., 2015). A small number of the events observed from the ground and on aircraft have been identified as TGFs (Belz et al., 2020; Bowers et al., 2017; Dwyer et al., 2004; Enoto et al., 2017; Hare et al., 2016; Smith et al., 2011; Wada, Enoto, Nakamura, et al., 2019). Events due to rocket-triggered lightning have also been observed with marked similarity to the natural events produced in association with natural lightning leaders (Dwyer et al., 2004; Saleh et al., 2020). Satellite-detected TGFs are predominantly correlated with upward-directed intracloud

(IC) lightning (Connaughton et al., 2010; Lu et al., 2010, 2011; Shao et al., 2010; Stanley et al., 2006) and ground-level events are generally associated with downward-directed cloud-to-ground (CG) lightning (Abbasi et al., 2017; Pleshinger et al., 2019; Tran et al., 2015).

At ground level, many of the observed events consist of X-rays at energies mainly below 250 keV (Dwyer et al., 2004), although energies exceeding 10–20 MeV have been detected in a few ground-level events (Bowers et al., 2017; Enoto et al., 2017; Tran et al., 2015; Wada, Enoto, Nakamura, et al., 2019). X-rays and gamma-rays of these energies are produced by bremsstrahlung from energetic electrons presumably accelerated to relativistic energies via a relativistic runaway electron avalanche (Gurevich et al., 1992). The avalanche is seeded either by a relativistic feedback mechanism (Dwyer, 2012; Dwyer et al., 2008) or by cold runaway acceleration in the intense field at the tip of an individual lightning leader (Babich et al., 2015; Carlson et al., 2010; Celestin & Pasko, 2011; Xu et al., 2012).

Electric fields in thunderstorms are created when vertical moisture advection rises within updrafts to the mixed-phase cloud isotherm between approximately −10°C and −40°C, with specific altitudes dependent on the environment. Within the turbulent updraft, mixed-phase cloud particles of supercooled water, ice crystals, and graupel collide, thereby exchanging electric charges. Generally, lighter ice crystals rise within an updraft creating a main positive charge at the upper region of the cloud, while heavier graupel descend creating a main negative charge in the center, with a weaker positive charge accumulating in the lower portion of the cloud, leading to an idealized "tripole" charge structure (Emersic & Saunders, 2010; MacGorman & Morgenstern, 1998; Saunders, 2008). The magnitude of the electric field and specific cloud charge structure vary based on the depositional growth of cloud particles (Dahl et al., 2011; Emersic & Saunders, 2010) and thunderstorm structures, which are determined by atmospheric properties: height of tropopause, ambient air temperature, wind shear, liquid water density, and velocity of updrafts (Dash & Wettlaufer, 2003; Saunders, 2008). The analysis of gamma-ray-producing thunderstorms can be expected to provide useful data about the electric fields and related thundercloud properties.

From the point of view of the analysis of thunderstorms producing X-ray and gamma-ray events, ground-based observations have advantages over space-based experiments in that they are closer to the storms, their field of view is narrower, and the instruments are stationary, constantly monitoring the same region(s). To our knowledge, there have been no systematic analyses of the thunderstorms associated with ground-level events. From space, although thousands of TGFs have been collectively detected by RHESSI, Fermi, AGILE, and ASIM, only a fraction have been geolocated to individual sferics (Connaughton et al., 2010, 2013; Lindanger et al., 2020; Mailyan et al., 2018, 2020; Østgaard et al., 2015; Roberts et al., 2018; Smith et al., 2016). Even fewer have been analyzed together with the thunderstorms producing them. In the most extensive thunderstorm analyses to date, Chronis et al. (2016) examined weather radar of 24 geolocated Fermi TGF events, concluding TGFs in this sample consistently occurred adjacent to high-altitude regions in the storms; and Ursi et al. (2019), based on a study of 278 TGFs detected by RHESSI, AGILE, and Fermi, concluded that the thunderstorms with TGFs had characteristics generally similar to those of storms without TGFs. Additional analyses of atmospheric conditions for TGF-producing thunderstorms report an apparent connection to high-altitude thunderstorms (Lu et al., 2010; Smith et al., 2010; Splitt et al., 2010; Ursi et al., 2019), a propensity for higher cloud liquid and ice content (Barnes et al., 2015; Fabró et al., 2015; Ursi et al., 2019) or increased convective available potential energy (Fabró et al., 2015; Splitt et al., 2010). Ursi et al. (2019) demonstrated that TGFs tend to occur within 5 min of the peak in lightning activity, and Shao et al. (2010) and Cummer et al. (2014, 2015), found that TGFs tended to be seen in association with the development of long, high-altitude leaders, suggesting a connection with the peak in the strength of the updraft and the maximum electrification. In contrast, Smith et al. (2010) found a correlation with the decreasing stage of the lightning peaks. Two studies reported TGFs originating from organized tropical systems, one from the eyewall of Hurricane Patricia in 2015 (Bowers et al., 2018) and the other originating from a rain band in Tropical Storm Andrea in 2013 (Chronis et al., 2016). Varying sample sizes, detection methods, and availability of atmospheric data complicate the ability to form concrete conclusions on the atmospheric characteristics required to produce TGFs.

The TGF and Energetic Thunderstorm Rooftop Array (TETRA I and II) is a ground-based detection array based out of Louisiana State University (LSU). TETRA I was in operation from 2010 to 2013, detecting 28 X-ray/gamma-ray events associated with lightning activity within 8 km and 5 min of each

Figure 1. TETRA-II array locations.

event (Ringuette et al., 2013). Lightning data at this time were insufficient for geolocation via sferic associations, limiting comprehensive thunderstorm analysis. The upgraded TETRA-II has been in operation since 2015, and in the following four years has reported results from 22 events, 20 of them associated with sferics from nearby lightning (Pleshinger et al., 2019). (A total of 58 events have been recorded by TETRA-II through the end of 2020. The remaining TETRA-II events will be discussed in an upcoming paper.) Of the 22 initial TETRA-II events, 20 were accompanied by a nearby lightning strike at distances ranging from 0.2 to 6.8 km, with the associated sferic occurring between 10 µs and 1.3 ms after the beginning of the gamma-ray event and typically within ∼100 µs of the end of the event, supporting the argument that these events were produced during the later stages of the lightning step leader process. About 2/3 of the events had a characteristic time structure, with the signal rising gradually over the typical 100 µs–1.75 ms duration of the X-ray/gamma-ray emission (average duration ∼800 µs), before abruptly ending at the time of the associated sferic. This suggests either that (a) the gamma-rays were typically produced by individual downward-moving leaders approaching the detector, resulting in detected count rates rising with decreasing distance due to decreasing atmospheric attenuation and increasing solid angle to the detectors (Pleshinger et al., 2019) or (b) that the bulk of the gamma-ray emission occurred during the last few hundred meters of the leader channel propagation to the ground (Dwyer et al., 2004; Saleh et al., 2020). Most of the remaining events had a relatively symmetrical time structure with average duration closer to 200 µs. The durations of the events are given in Table 2 in Pleshinger et al. (2019). The single exception was Event 170707 observed in Baton Rouge, in which the signal rose abruptly and then decayed away over ∼5 ms. The TETRA-II events have the relatively soft energy spectra expected from lightning leader-associated events rather than the harder and more intense TGFs and appear to be similar to the ground-level events due to lightning leaders reported by Moore et al. (2001) and others. Time profiles of the individual TETRA-II events can be found at https://tetra.phys.lsu.edu.

Here, we present an analysis of the characteristics of the thunderstorms associated with these first 22 TETRA-II events associated mainly with lightning leaders. The TETRA-II and associated lightning and weather data are described in Section 2. In Section 3, electrical and/or atmospheric characteristics associated with the TETRA-II gamma-ray events are presented. Conclusions are presented in Section 4.

2. Data and Methods

2.1. TETRA-II Gamma-Ray Event Data

TETRA-II consists of detectors on the campus of LSU in Baton Rouge, Louisiana; the University of Puerto Rico (UPR) in Utuado, Puerto Rico; the Centro Nacional de Metorología de Panamá (CENAMEP) in Panama City, Panamá; and the Severe Weather Institute-Radar and Lightning Laboratories (SWIRLL) at the University of Alabama in Huntsville, Alabama (Figure 1 and Table 1). (The Alabama detectors saw no events in 2 years of operation and have been removed.)

Each array consists of multiple detector boxes, each box containing six $25.4 \times 2.5 \times 2.5$ cm^3 bismuth germanate (BGO) scintillators sensitive to energies between 50 keV and 6 MeV and viewed by photomultiplier tubes. Absolute timing is derived from a GPS signal every second and a 20 MHz oscillator which provides timing of individual phototube pulses

Table 1
Detector Locations and Events Detected

Array location	Duration (years)	Events
Baton Rouge	3	12
(30.41°, −91.17°)		
Panama City	3	9
(9.00°, −79.58°)		
Utuado	2.5	1
(18.25°, −66.72°)		
Huntsville	2	0
(34.72°, −86.64°)		

Table 2
List of TETRA-II Events and Corresponding Geolocations via Sferic Association

Event	Location	Time (UTC)	Counts	Duration	Lat	Lon	Source	Type	Peak current	Distance
160427	Baton Rouge	16:49:25.418	19	100	30.4100	−91.1889	NLDN	−CG	−111.4	1.0
160919	Utuado	18:09:32.762	183	800	18.2763	−66.7136	GLD360	−pol	−16.6	2.6
170307	Baton Rouge	23:34:30.446	169	700	30.4138	−91.1834	NLDN	−CG	−66.4	0.5
170325a	Baton Rouge	15:47:15.270	73	500	30.4114	−91.1774	NLDN	−CG	−22.3	0.2
170325b	Baton Rouge	16:02:12.737	29	450	30.4092	−91.1774	NLDN	−CG	−51.7	0.4
170325c	Baton Rouge	16:02:12.918	61	250	30.4096	−91.1770	NLDN	−CG	−32.6	0.4
170601	Panama City	01:15:24.179	23	850	9.0320	−79.6289	GLD360	−pol	−51.1	5.9
170624a	Baton Rouge	19:34:50.268	203	1,150	30.4096	−91.1770	NLDN	−CG	−43.5	0.4
170624b	Baton Rouge	19:34:50.475	133	400	30.4086	−91.1777	NLDN	−CG	−32.7	0.5
170624c	Baton Rouge	19:34:50.364	48	100	30.4088	−91.1769	NLDN	−CG	−36.6	0.5
170707	Baton Rouge	22:25:51.186	113	5,950	*	*	*	*	*	*
170810a	Panama City	14:34:01.703	91	1,350	8.9968	−79.5817	GLD360	−pol	−139.5	0.6
170810b	Panama City	14:34:01.684	19	350	*	*	*	*	*	*
171018a	Panama City	17:43:46.565	97	1,550	9.0044	−79.6077	GLD360	+pol	55.9	2.5
171018b	Panama City	17:45:31.545	34	900	8.9902	−79.6088	GLD360	−pol	−67.1	2.9
171103	Panama City	19:34:30.382	25	350	9.0490	−79.5501	WWLLN	*	*	6.5
171204	Panama City	17:54:50.349	24	1,750	8.9984	−79.6166	GLD360	−pol	−22.5	3.5
180605	Panama City	11:59:21.008	44	650	9.0052	−79.6464	WWLLN	*	*	6.8
180815	Baton Rouge	22:56:43.222	56	950	30.4097	−91.1824	NLDN	−CG	−25.6	0.5
180817	Baton Rouge	13:51:59.767	45	650	30.4132	−91.1834	NLDN	−CG	−95	0.5
181022	Panama City	21:54:00.386	89	1,300	8.9759	−79.5921	GLD360	−pol	−113.8	1.1
190315	Baton Rouge	08:11:21.506	99	500	30.4218	−91.169	NLDN	-IC	−8.7	1.3

Note. *Indicates no data. Adapted from Pleshinger et al. (2019) Events 170707 and 170810b are not correlated to individual sferics and, therefore, have no coordinate values. Gamma-ray data including location, timestamp, counts (number of photons), and duration (μs) are listed for the gamma-ray events. Sferic data include coordinates, lightning data source, type of lightning, peak current (kA), and distance (km). In the column "Type," "pol" indicates stroke polarity (− or +).

to 50 ns. Currently, Utuado houses 59 BGO units, Panama City 29, and Baton Rouge 11. The detectors and initial results are described in detail in Pleshinger et al. (2019).

Event candidates are identified by binning the entire day into 2 ms bins and selecting events exceeding 20 standard deviations above the daily average background. Once a gamma-ray event is found, the time stamp is compared with the Global Lightning Data set (GLD360), National Lightning Detection Network (NLDN), and World-Wide Lightning Location Network (WWLLN) lightning catalogs, searching for a strike within 8 km of the detector location and 5 s of the trigger time (Pleshinger et al., 2019). If two lightning strokes satisfy this criterion, the lightning stroke with the closer coincidence in time is taken as the stroke associated with the X-ray/gamma-ray event. The two exceptions to this rule are 170305 and 170810a, where the NLDN or GLD360 distance is 0.5–0.6 km, the WWLLN distance is 3–6 km, and the timing is within 20 μs. In these cases, preference is given to NLDN or GLD360 because of the superior position resolution compared to WWLLN. Of the 22 TETRA-II events detected, 20 have a sferic detection within 7 km and 1.3 ms of the beginning of the gamma-ray event. In every case, the sferic is reported after the start of the gamma-ray event, usually within ∼100 μs of the end of the event. A list of the TETRA-II events and corresponding sferic associations is provided in Table 2 and supporting information Table S1. Events are labeled numerically by detection date in the format: year-month-day. (UTC is 5 h ahead of Utuado, 4 h ahead of Panama, and 5–6 h ahead of Baton Rouge depending on whether Daylight Savings Time is in effect.) It should be noted that Table 2 differs slightly from the tabulation in Pleshinger et al. (2019): Event 180915, the weakest event

analyzed in Pleshinger et al. (2019), was not associated with a nearby storm and has been removed; and the cold weather event 190315 has been added.

An important caution should be noted about the distances to the lightning noted in Table 2. The location accuracy of the three lightning networks varies considerably from <500 m for NLDN (Cummins, Krider, & Malone, 1998; Cummins, Murphy, et al., 1998; D. Zhang et al., 2016) to ~2 km for GLD360 (Said & Murphy, 2016) to >5 km for WWLLN (Abarca et al., 2010; Hutchins et al., 2012; Rudlosky & Shea, 2013). Although the values for lightning distance in Table 2 suggest that events in Panama are more distant from the TETRA-II detectors than in Baton Rouge, this may be an effect due to the relatively poorer location accuracy of GLD360 and WWLLN in Panama compared to NLDN in Baton Rouge.

2.2. Lightning Rate and Lightning Jumps

Lightning stroke (sferic) data are provided by GLD360, NLDN, and the University of Washington's WWLLN. GLD360 is a ground-based network of sensors providing global-scale geolocation using time-of-group-arrival (TOGA) with a minimum of three sensors and magnetic direction-finding technology. GLD360 detects mainly CG return strokes with ~80% flash detection efficiency compared to NLDN (Said & Murphy, 2016). Also owned and operated by Vaisala, NLDN consists of more than 100 ground-based sensors over the contiguous United States, also utilizing TOGA and magnetic direction finding. NLDN has a detection efficiency ~90% for flashes and 60%–80% for individual strokes (Cummins, Murphy, et al., 1998). Both GLD360 and NLDN provide data regarding polarity (−/+) and lightning current; lightning type (IC/CG) identification is provided by NLDN. WWLLN consists of over 70 sensors worldwide, supplying geolocation information using TOGA with a minimum of five sensors.

Electric fields associated with thunderstorms have been estimated to extend up to 15 km from the cloud edge, decreasing in magnitude with distance (MacGorman & Morgenstern, 1998; Merceret et al., 2008). Gamma-rays with energies between 50 keV and 6 MeV undergo photoelectric, Compton, and pair production interactions and do not travel more than a few km in air at ground level. To limit analysis to thunderstorms with fields potentially strong enough to generate electron acceleration and close enough so that the photons might be able to propagate to the detector, and at the same time allow for the position resolution of the lightning networks, only thunderstorms with lightning within an 8 km distance from the TETRA-II detector locations are considered. Lightning activity is considered to be associated with an event-producing thunderstorm provided lightning occurs within 8 km and lightning activity persists with no gaps in excess of 30 min. All lightning calculations are based on this radius and do not represent the entire thunderstorm. When a lapse in lightning activity exceeds 30 min, a new thunderstorm cell is assumed.

Three primary lightning/thunderstorm characteristics (lightning frequency type, thunderstorm phase, and lightning frequency distribution) are based on lightning discharge rate, calculated using one-minute binned lightning beginning at the onset of the first stroke.

1. *Binary lightning frequency type (high-frequency, low-frequency).* Thunderstorms are considered high frequency when the average full-storm discharge rate exceeds 5 strokes/min and/or the peak 1-min stroke rate exceeds 20 strokes/min (Gatlin & Goodman, 2010) based on the NLDN, GLD360, or WWLLN observations.
2. *Binary thunderstorm phase (mature/off-peak).* Storms are classified as off-peak or mature based on whether the ratio of stroke rate at the time of event to the average stroke rate over the previous 15 min is <0.2 for off-peak or >0.2 for mature phase (Miller et al., 2015).
3. *Lightning frequency distribution.* Lightning jumps denote abrupt increases in lightning stroke rate (Williams et al., 1999) and are used to identify regions of updraft intensification and potentially severe weather and to indicate electric fields at the limit of field breakdown (Schultz et al., 2015). Jumps are defined as intervals when the lightning stroke rate per minute exceeds the 10-min running average by at least 2 standard deviations (Gatlin & Goodman, 2010). Low-frequency thunderstorms (average <5 strokes/min) are excluded from the jump analysis.

Table 3
Storm Severity Classification

Classification	Wind speed (km/h)	Hail size (in)
Severe	>93	>1
Approaching severe	>64	0.5–1
Non-severe	<64	<0.5

Note. Adapted from National Weather Service, 2019.

2.3. Weather and Next Generation Radar Data

Thunderstorms are first classified by type (single-cell, squall line, multi-cell, and supercell). Classifications are made by analyzing the number of individual cells within a parent storm, the size and shape of parent storm combined with a classification of strength (severe, approaching severe, and non-severe; Table 3). A storm's severity is classified based on whether it satisfies either a minimum wind speed or minimum size of hail observed at the ground as observed by official severe weather alerts issued by the US National Weather Service (NWS). Ambient air temperature and storm severity data for the Baton Rouge and Utuado analyses are retrieved from the National Weather Service. For Baton Rouge, the Baton Rouge Metropolitan Airport, Ryan Field (KBTR, ~15 km from TETRA-II) is used; and for Utuado, the San Juan, Luis Muñoz Marín International Airport (TJSJ, ~100 km from TETRA-II) is used.

NEXRAD radar data are used to provide quantitative convective characteristics of thunderstorms associated with TETRA-II events. NEXRAD provides reflectivity and reflectivity-derived data from a network of dual-polarization radar towers in the United States and United States territories. NEXRAD products are used in conjunction with lightning sferic data to analyze the structure and convective properties of thunderstorms associated with TETRA-II events. However, since Panama does not fall within the NEXRAD monitoring zone and external radar data for this location are unavailable at this time, only the Baton Rouge and Utuado TETRA-II data are analyzed in conjunction with NEXRAD. Base reflectivity (BR) and three derivatives of BR are utilized: echo tops (ETs), vertically integrated liquid density (VILD), and the hail detection algorithm (HDA). Radar sweeps range from 2 to 10 min, depending on the product. Three radar towers are utilized for Baton Rouge coverage: KLIX (New Orleans), KLCH (Lake Charles), and KPOE (Fort Polk), at distances 175, 200, and 250 km, respectively, from the TETRA-II location at LSU, providing 12 volume coverage patterns (VCP) at altitudes up to 30 kft above ground level. One tower provides data for Utuado: TJUA (San Juan), located 109 km from the TETRA II sensor with VCP radar scans up to 60 kft above ground level. Data are provided by the National Oceanic and Atmospheric Administration and viewed by the GR2Analyst program provided by Gibson Ridge Software, LLC.

1. *BR* measures echo intensity (reflectivity) of an emitted radar pulse, measured in decibels relative to Z (dBZ), where Z is the reflectivity factor of a returned pulse. This product is used to interpret parent storm type, individual cell phase, structure, location, vertical extent, updraft/downdraft regions, and precipitation cores.

2. *ETs* represent the maximum vertical height of BR exceeding 18.5 dBZ and is used as an estimation of cloud top height and to infer the strength of updraft regions. Cloud electrification and lightning production require updrafts to persist within mixed-phase cloud altitudes, that is, altitudes where temperatures allow for the presence of both supercooled water and ice (generally between −10°C and −40°C). Mixed-phase altitudes vary based on environmental lapse rate. Panama City and Utuado are at tropical latitudes with little temperature variation and extended troposphere altitudes; while Baton Rouge lapse rates vary seasonally.

3. *VILD* is a measure (g/m^3) of BR converted into an equivalent liquid water content value relative to ETs and is used to estimate the water/ice content of a column of air. In this study, it is used to infer areas of updraft intensification and regions of potential cloud electrification via frictional mixing. Thunderstorm cells with high reflectivities relative to their height indicate high ice flux and high velocity moist updrafts (Amburn & Wolf, 1997).

4. *HDA* is a NEXRAD product derived from BR, ET, and VILD and used as a quantitative estimator of hail cell regions and hail size. Potential hail cells are identified as regions with BR >45 dBZ within mixed-phase altitudes. Identified hail cells are then categorized according to the Probability of Hail (POH) being produced with diameters >0.5 in or Probability of Severe Hail (POSH) >1 in (Witt et al., 1998). The presence of hail cells is related to updraft velocity relative to precipitation content and is commonly used as an indicator of thunderstorm strength and updraft intensity (Houze, 2014; Pruppacher & Klett, 2010).

To account for the spatial uncertainty of lightning data and the 2–10 min time resolution of NEXRAD radar sweeps, for each event an interpolated median (IM) for BR, ET, and VILD is calculated from the values

of all pixels or pixel fractions within 3 km of the lightning location (Aggarwal et al., 2010). Radar scans associated with the interpolated radar products occur within 3 min of each TETRA-II X-ray/gamma-ray event. The offset times for individual events are as follows: 160427 (9 s), 160919 (~1 min), 170307 (2.5 min), 170325a (20 s), 170325bc (~2 min), 170624abc (20 s), 180815 (~3 min), 180817 (~3 min), 190315 (~1 min), respectively.

3. Results and Discussion

3.1. Spatiotemporal Distribution

Over its first ~3.5 years of operation (October 2015–March 2019), TETRA-II recorded the majority of its events in Baton Rouge (12) and Panama (9). Only one event was detected in Utuado and none in Huntsville. Average rates of lightning are 18 flashes km^{-2} yr^{-1} in Baton Rouge, 35.1 fl km^{-2} yr^{-1} in Panama City, 43 fl km^{-2} yr^{-1} in Utuado, and 9 fl km^{-2} yr^{-1} in Huntsville (Albrecht et al., 2016), indicating overall lightning flash rate is not the main factor responsible for the differences. Although Huntsville and Baton Rouge are both classified as subtropical climates, monthly mean temperatures in Huntsville are, on average, 10°C cooler and mean annual relative humidity values are approximately 5% less than in Baton Rouge, again likely not solely responsible for the bulk of the Huntsville-Baton Rouge difference. Smith et al. (2010), Roberts et al. (2018), Albrechtsen et al. (2019), and Lindanger et al. (2020) have all reported an apparent tendency for TGFs to occur in coastal locations over inland locations, although the detailed reasons for this are not well understood. In the TETRA case, CENAMEP in Panama City is located 7 km inland from the Gulf of Panama; UPR in Utuado sits 24 km inland from the Atlantic Ocean; LSU in Baton Rouge is 100 km inland from the Gulf of Mexico; and SWRLL in Huntsville sits 650 km from the nearest coast. Since the TETRA-II events generally appear to be lightning-leader events rather than TGFs, it is not clear that the observed TGF correlation with coastal rather than inland locations is relevant. Nevertheless, the lack of events in Huntsville may be due to its distance from the coast. This does not explain the small number of events in Utuado, however. Finally, Huntsville and Utuado are located at higher elevations (180 and 250 m) and are both surrounded by mountainous terrain, whereas Baton Rouge and Panama City have elevations of 17 and 2 m, respectively.

Events are produced in thunderstorms with ground-level ambient air temperatures ranging from 13°C to 25°C with forward speed of storms ranging from 5 to 39 km/h. Events occurring in cold frontal thunderstorm systems occur exclusively in Baton Rouge due to the influence of continental climate, in contrast to the tropical climate conditions sampled in Utuado and Panama and by the satellite-borne TGF detectors.

The diurnal distribution of TETRA-II events (Table 2) shows a tendency for events to occur in late morning through early evening, with only three events occurring between local hours of 9:00 p.m. and 9:00 a.m. In addition, the seasonality of TETRA-II events roughly coincides with peak seasonal distribution of thunderstorms for each location. This is similar to the results of Albrecht et al. (2016), whose high-resolution hourly mean lightning climatologies confirm a diurnal tendency for late afternoon and evening thunderstorms at each location, typical for subtropical and tropical climates. It is also similar to the results of Splitt et al. (2010), Roberts et al. (2018), and Maiorana et al. (2020), who have shown that TGFs recorded by RHESSI, Fermi GBM, and AGILE also tend to follow the local lightning frequency pattern.

3.2. Lightning Frequency Classification

As shown in Table 2, TETRA-II events occurred in 15 individual thunderstorms, 4 of which produced multiple gamma-ray events (170325abc, 170624abc, 170810ab, and 171018ab). Two events were not associated with an individual lighting stroke (170707 and 170810b). Event 170707 in Baton Rouge was a long-duration outlier event that did not occur within 8 km of a thunderstorm, although lightning strokes were recorded from a severe storm at a distance 11 km from TETRA-II. Event 170707 is discussed in more detail in Section 3.4. Event 170810b in Panama occurred 19 ms prior to 170810a, but did not have an associated sferic. In the cases of both 170707 and 170810b, the non-observation of an associated sferic is consistent with the 60%–80% detection efficiency of NLDN and GLD360 for individual strokes.

Table 4
Lightning Frequency Within 8 km of TETRA-II Events

Event	Source	Storm duration (min)	Peak stroke rate (min^{-1})	Average stroke rate (min^{-1})	Frequency
160427 (BR)	NLDN	91	131	20	High
160919 (Ut)	GLD360	96	131	5	High
170307 (BR)	NLDN	116	66	13	High
170325abc (BR)	NLDN	416	106	11	High
170601 (Pan)	GLD360	148	26	8	High
170624abc (BR)	NLDN	93	195	46	High
170707 (BR)	–	–	–	–	
170810ab (Pan)	GLD360	9	3	<1	Low
171018ab (Pan)	GLD360	137	118	17	High
171103 (Pan)	WWLLN	61	4	<1	Low
171204 (Pan)	GLD360	187	15	1.5	Low
180605 (Pan)	WWLLN	112	7	<1	Low
180815 (BR)	NLDN	139	71	22	High
180817 (BR)	NLDN	102	38	6	High
181022 (Pan)	GLD360	132	7	<1	Low
190315 (BR)	NLDN	16	5	<1	Low

Note. The Values in Table 4 are Based on GLD360 or WWLLN Stroke Rates in Utuado and Panama, and on NLDN in Baton Rouge.

Events were observed during storms corresponding to 10-min average stroke rates ranging from <1 to 46 stroke/min (Table 4). Peak (1-min) stroke rates ranged from 3 to 195/min. As described in Section 2.2, a new thunderstorm cell is defined to start when lightning resumes following a 30-min lapse in lightning activity. The time over which the thunderstorm persists within close proximity to TETRA-II (measured from the first to the last stroke in the cell within the 8 km TETRA-II radius) ranged from 9 min to nearly 7 h; this is listed in Table 4 as "Storm duration." We emphasize that the restriction to the region within 8 km of the TETRA-II location is intended to focus on the region of the storm where the updraft intensification and subsequent electrification is close enough to the detector location to have a potential impact on the observed X-ray/gamma-ray signal; our conclusions do not necessarily apply to the entire storm.
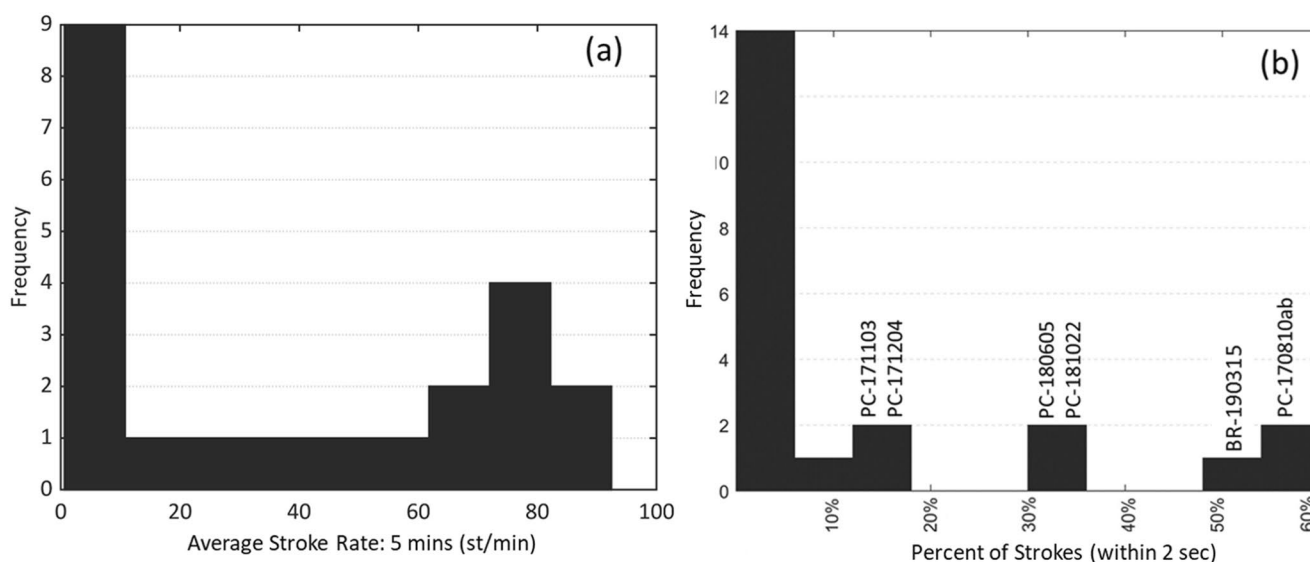
3.2.1. Low Stroke Rate Thunderstorms

About 7 of the 22 TETRA II events are classified as associated with low lightning frequency thunderstorms with <5 strokes/min. All but one low stroke frequency storm occurred in Panama. It should be noted that the detection efficiency for the lightning networks differs from network to network, for IC versus CG lightning, for strokes versus flashes, for one location versus another, as a function of peak current and time of day, and as a function of calendar date as networks are upgraded. Said and Murphy (2016) have compared the GLD360 detection efficiency after its 2015 processing algorithm upgrade to that of NLDN and found an overall relative GLD360-to-NLDN detection efficiency for CG flashes over the continental US ranging from 85% at night to 76% during the local afternoon hours of peak activity. Rudlosky et al. (2017) quote a GLD360 flash detection efficiency (using data for 2014 after reprocessing with the upgraded 2015 software algorithms) ranging from 48.7% over all land areas globally to 65.8% over the US. The average stroke rate for storms producing TETRA-II events and detected by NLDN in Baton Rouge (Table 4) is 17 strokes/min; in Panama, the average rate from Table 4 for the five storms detected by GLD360 is 5/min. Even accounting for the different efficiencies of GLD360 in Panama versus NLDN in Baton Rouge, the conclusion appears to be that the TETRA-II events in Panama occur in storms with less lightning than in Baton Rouge.

Figure 2a shows the distribution of stroke rates per minute averaged over 5 min at the times of all TETRA-II events. Nine of the 22 events occurred when the 5-min average stroke rate was <10 strokes/min. With the exception of 171018a and b and 170601, all Panama event-producing thunderstorms exhibited lightning rates <2 strokes/min. Conversely, only one low stroke frequency storm occurred in Baton Rouge, suggesting that different thunderstorm types produced events in Panama and Baton Rouge.

Figure 2b shows the fraction of strokes in the 5-min window that occurred within 2 s of the gamma-ray event. In the majority of cases, the fraction of lightning strokes within 2 s was less than 15%. However, in the six storms classified as low-stroke-rate storms (full-storm stroke rate <5 strokes/min), the fraction of lightning within 2 s was >15%; these six low-stroke-rate storms are labeled in Figure 2b. In other words, even in storms with overall low stroke rates, TETRA-II X-ray/gamma-ray events occurred at times of rapid intensification of the electric field. Three events are found at the upper end of the distribution: In event 190315, 50% of all lightning occurred within 1 s and 0.5 km of each other; and in events 170810ab, 60% of the lightning occurred within 2 s and no additional lightning occurred within several minutes. A high fraction of short-term to longer-term lightning suggests that the magnitude of the electric field was increasing rapidly, leading to the initiation and/or increase of electron acceleration.
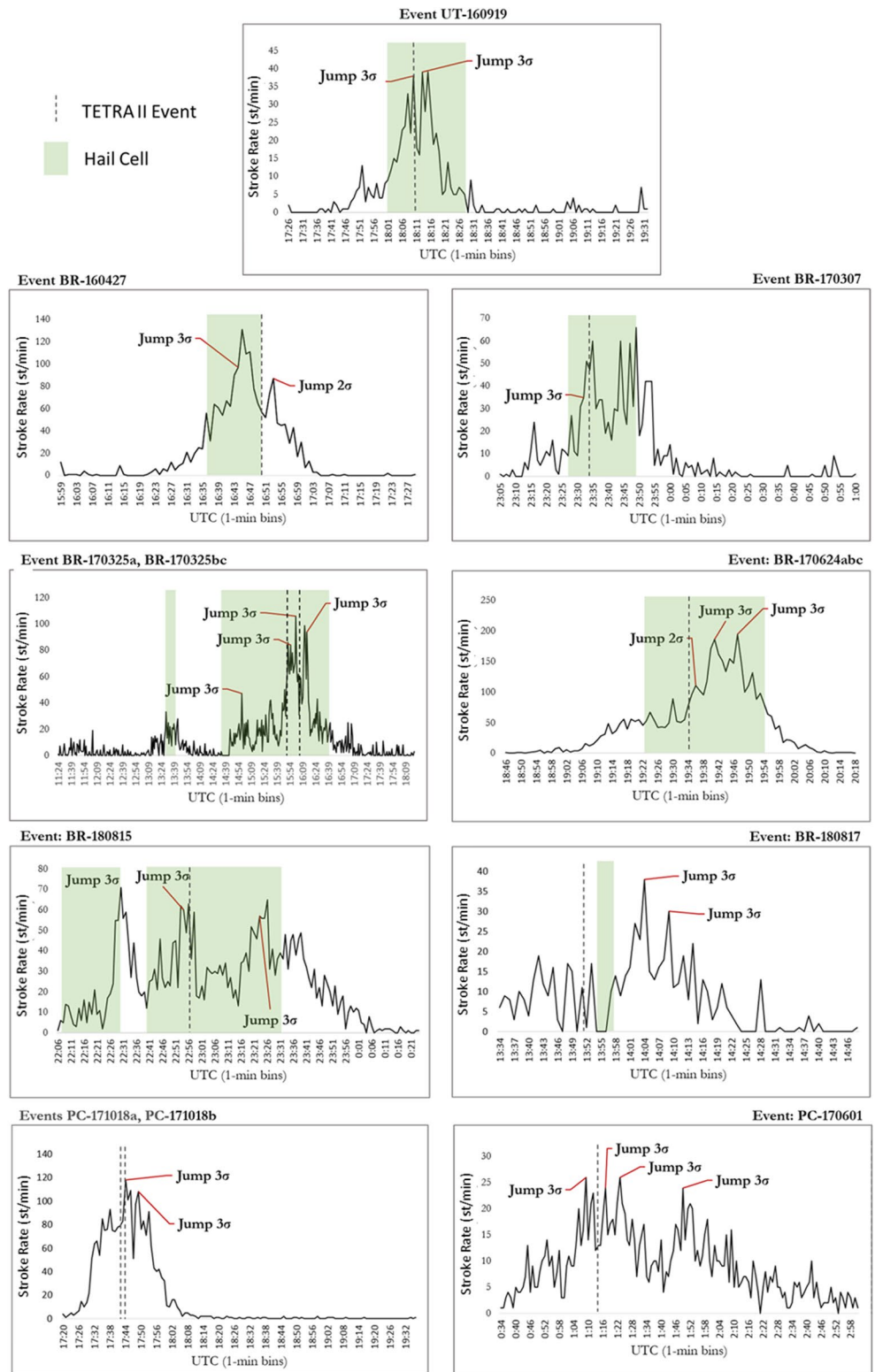
Figure 2. (a) Distribution of the 5-min lightning stroke rate in storms with TETRA-II events. (b) Fraction of strokes that occur within 2 s. Low stroke rate thunderstorms are common in (a), whereas in (b), a significant fraction of storms (especially low-stroke-rate storms) have brief intervals with high rates (i.e., periods of rapid intensification).

3.2.2. High Stroke Rate Thunderstorms

In contrast to the 7 low stroke rate events, 14 TETRA-II events were detected in high-stroke-rate thunderstorms with lightning stroke rate >5/min. Observed lightning jumps are used to characterize thunderstorm electrification. Figure 3 shows the distribution of lightning stroke rate and presence of jumps for the storms with >5 strokes/min. In all cases, the gamma-ray events occur within 5 min of a 2–3σ lightning jump, again indicating that events occur during or shortly after intensification of the updraft. Lightning jumps are grouped by thunderstorm; that is, multiple events within a single thunderstorm are analyzed and displayed together in Figure 3.

Hail cells identified by NEXRAD's HDA are included in the lightning jump analysis (Figure 3) based on the relationship between lightning and hail production. Panama City events are not within the NEXRAD-monitoring region and are thus excluded from the hail cell analysis. Table 5 lists the hail cells closest in time to each event, their associated size, POH, and the POSH. With the exception of the single low-stroke-rate cold weather event in Baton Rouge (190315), all thunderstorms in the NEXRAD monitoring zone had hail cells present within ~8.5 km and 3 min of the gamma-ray bursts. Five of these cells were accompanied by the potential of severe hail (POSH ≥ 10). The presence of large hail indicates the system has a strong updraft, and this strong updraft enhances the electrification of the cell due to increased mixed-phase particle collisions and resulting charge separation. Lateral distance between event geolocations and the nearest hail cell range from <1 km to approximately 8.5 km, with slightly over half occurring <5 km from the events. In most cases, hail cell regions are detected for several minutes before TETRA-II events (Figure 3). This is consistent with the finding of Changnon (1992), who showed that lightning begins during hail formation aloft and that hail aloft precedes lightning by several minutes and can occur several kilometers from the hail cell.

The two severe multicell thunderstorms producing multiple events (170325abc and 170624abc) correspond to hail cells lasting for several minutes and up to a few hours surrounding the events. Event 170707 is included in Table 5 because there is a storm 8.5 km away. Since this is beyond the standard 8 km limit for the analysis, and there is no nearby lightning associated with 170707, it is not included in the remaining analysis but is discussed separately in Section 3.4.

Figure 3. Lightning jumps and hail within high lightning frequency thunderstorms. Vertical dashed lines indicate the times of TETRA-II X-ray/gamma-ray events. Green bars indicate duration of hail cells within 8 km of TETRA-II events. No hail data exist for Panama City events (bottom row). Multi-cell thunderstorms have multiple lightning jumps as cells reproduce within the 8 km radius. Smaller and shorter-lived thunderstorm cells have fewer lightning jumps within 8 km.

Table 5
Hail Occurrence in TETRA-II Events in Baton Rouge and Utuado

Event	Time delay (min)	Distanc (km)	Hail diameter (in)	POH	POSH	Cell ID
160427	0.25	6.12	0.5	80	0	KLIX:F5
160919	1.1	5.55	1	90	20	TJUA:NA
170307	0.5	1.66	0.5	80	10	KPOE:R4
170325a	0.25	0.82	1	90	70	KLCH:V7
170325b	0.01	4.5	0.5	80	20	KLX:I1
170325c	0.01	4.5	0.5	80	20	KLX:I1
170624a	1.83	4.38	0.75	90	0	KLCH:P9
170624b	1.83	4.38	0.75	90	0	KLCH:P9
170624c	1.83	4.38	0.75	90	0	KLCH:P9
170707	2	8.54	0.75	80	0	KLIX:NA
180815	0.01	3.11	0.5	90	0	KPOE:C5
180817	3	7.76	0.5	80	0	KDGX:I8
190315	NA	NA	NA	NA	NA	KLIX:NA

Note. Time delay in minutes indicates time by which nearest NEXRAD scan with presence of hail precedes the gamma-ray event.

Table 6
Thunderstorm Classifications Based on NWS Classifications in Table 3

Event	Type	Strength	Speed (km/h)	Temp (°C)
160427	Squall	Non-severe	37	19.5
160919	Multi-cell	Severe	20	22.75
170307	Squall	Approaching severe	39	20
170325a	Squall	Severe	20	20
170325bc	Squall	Approaching severe	20.5	19.5
170624abc	Multi-cell	Severe	21	25
180815	Multi-cell	Non-severe	5.5	24.5
180817	Multi-cell	Non-severe	14.5	25
190315	Multi-cell	Non-severe	20	12.75

3.3. Thunderstorm Characteristics (NEXRAD)

Of the 13 TETRA-II events located within the NEXRAD-monitoring regions (Utuado and Baton Rouge), 12 have sferic associations from 8 individual thunderstorm systems, 2 of which produced multiple events (170325abc and 170624abc). Event-producing thunderstorm types include squall lines and multicellular thunderstorms of varying strengths, structures, and duration (Table 6). All events occur in the mature stage of thunderstorm development with updrafts of sferic-geolocated individual cells within mixed-phase cloud altitudes. There are no single-cell or supercell thunderstorms in this sample. Although supercell thunderstorms are not common at the latitudes of southern Louisiana and Puerto Rico, all locations are prone to frequent single-cell afternoon convective "pop-up" thunderstorms. The lack of single-cell storms associated with the TETRA-II gamma-ray bursts suggests that the electron acceleration and gamma-ray production are tied to the updraft duration and horizontal extent of the thunderstorm cells.

To illustrate storm structures, a two-dimensional (10 km × 10 km) vertical cross-section of BR centered on each NEXRAD-monitored event associated with a thunderstorm is shown in Figure 4. Three events—170624a, b, and c—occur within ~200 ms of each other and are shown together on the same figure. Similarly, 170810a and b occur within 20 ms and are shown as part of the same storm. Structures range from low-altitude cold weather convection (190315) to high-altitude, uniform cloud top deep convection (170325abc) to overshooting cloud tops (160919 and 170624abc), suggesting that events do not require a particular strength of storm.
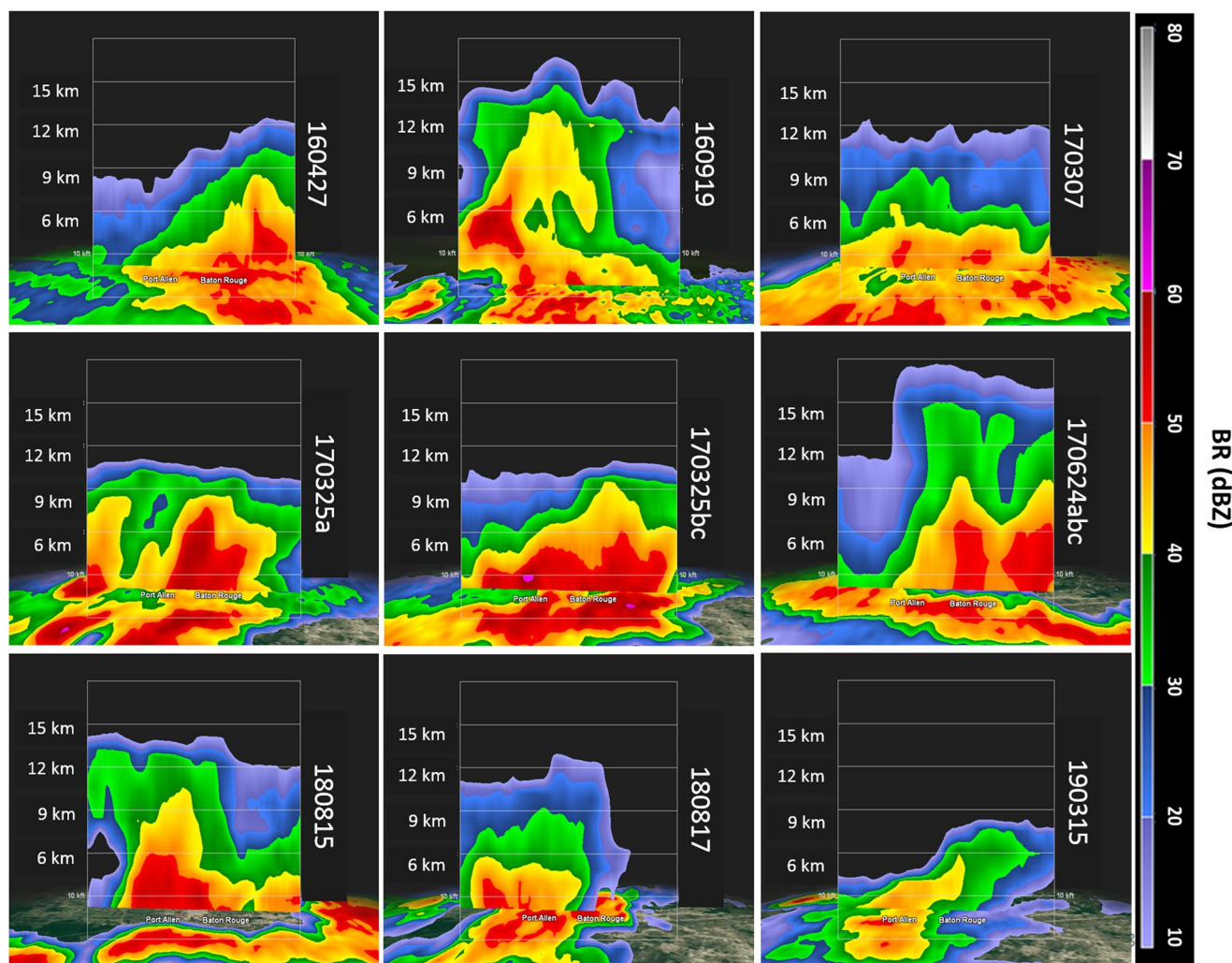
Table 7 shows IM, minimum, and maximum values for BR, ET, and VILD calculated for a radar sweep over a 3 km radius from the location of the associated lightning strike. Maximum cloud top altitudes range from 8.8 to 16.3 km. It is not clear that thunderstorms producing TGFs observed from space are the same storms as those producing the ground-level events seen by TETRA-II. Nevertheless, Splitt et al. (2010) found a tendency for RHESSI thunderstorm heights to range from 13.6 to 17.3 km; Chronis et al. (2016) reported maximum Fermi thunderstorm heights ranging from 12.1 to 17.6 km; and Ursi et al. (2019) found their sample of TGFs to occur above 15 km. Since there appears to be no apparent physical reason for TGFs to occur exclusively in higher altitude thunderstorms, Splitt et al. (2010) and Chronis et al. (2016) suggested a possible selection bias: that is, that the satellite instruments may preferentially detect high altitude events due to attenuation from events potentially produced at lower altitudes. A separate selection effect is presumably due to the fact that the events observed from space are mainly due to upward-moving IC strokes while the events seen from the ground are largely due to downward-moving CG strokes.

A similar result holds for the IM ET values. IM ET values in Table 7 range from 7.5 to 13.8 km with the interquartile range (shown below in Figure 5a) generally also above 7 km (i.e., within mixed-phase cloud altitudes). In contrast, Chronis et al. (2016) reported all Fermi TGFs had ETs between 10.0 and 16.1 km, again indicating that the storms associated with TETRA-II events have a tendency to occur at lower altitudes than the events seen from space; that is, the ground-level events may be intrinsically different from the TGFs seen from space. TETRA II events with ETs below 12 km are related to thunderstorms occurring in cooler temperatures, where the mixing layer is lower. The highest and lowest median ET correspond to the single Utuado event (160919) and the cold-weather event in Baton Rouge (190315), respectively.

Figure 4. 10 km × 10 km base reflectivity cross-sections of thunderstorms producing TETRA-II NEXRAD events. Scan time closest to event is displayed. Center of image is centered on TETRA-II location.
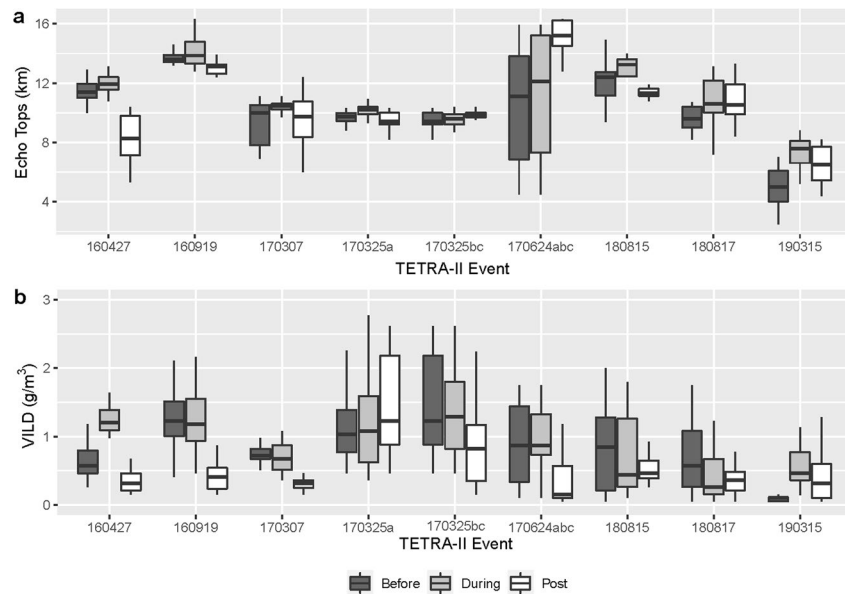
Table 7

Values of Radar Products for TETRA-II Events: Interpolated Median (IM), Minimum, and Maximum Values of BR, ET, and VILD

Event	BR (dBZ)			ET (km)			VILD (g/m3)		
	IM	Min	Max	IM	Min	Max	IM	Min	Max
160427	46.31	32.5	54.5	12.2	10.8	13.1	1.59	0.98	1.64
160919	49.50	37.5	60.5	13.8	12.8	16.3	1.05	0.26	2.16
170307	47.58	36	56	10.5	8.2	11.1	0.42	0.36	1.08
170325a	50.5	36.5	61.5	10.9	8.9	10.9	1.08	0.36	3.75
170325bc	53.07	44.5	60	9.7	8.7	10.4	1.29	0.46	2.62
170624abc	47.06	23	54	12.1	7.3	15.8	1.25	0.1	1.75
180815	48.81	26.5	56.5	13.2	7	14	0.44	0.1	1.8
180817	40.5	17	53.5	10.7	3.5	13.1	0.26	0.05	1.23
190315	37.25	14.5	51	7.5	3	8.8	0.46	0.14	1.13

The thunderstorm associated with event 190315 was the only low-altitude (8.8 km) thunderstorm in the sample. Additionally, it was the only NEXRAD thunderstorm to occur in the absence of a detectable hail cell (Table 5); it was the only Baton Rouge event characterized by low lightning frequency (Table 4); and it had the lowest bounds of ET and VILD values in the sample (Table 7). Compared to the other thunderstorms in the sample, 190315 is the weakest thunderstorm associated with a TETRA-II event. It is interesting to note that, although 190315 is the only low-temperature low-altitude winter storm in the TETRA-II sample, winter thunderstorms in Japan have been shown to produce both ground-level terrestrial gamma flashes and neutron events (Bowers et al., 2017; Wada, Enoto, Nakazawa, et al., 2019).

Higher VILD is correlated with hail and the presence of high reflectivity cores and strong updrafts. Ranges between minimum and maximum VILD values quantify the extent of the VILD cores. TETRA-II events occur during thunderstorms with median VILD values ranging from 0.3 g/m³ to approximately 1.6 g/m³ and with a lower bound to the maximum

Figure 5. Box and whisker plot of ET (top) and VILD values (bottom) within 3 km radius for the radar scans immediately before, during, and after each of the TETRA-II events at Baton Rouge and Utuado. Vertical whiskers represent the minimum and maximum ET values. Boxes represent the 25% to 75% quartiles, with a horizontal line denoting median values. Outlier points (points sitting more than 1.5 times the interquartile range above the upper quartile and below the lower quartile) are not shown.
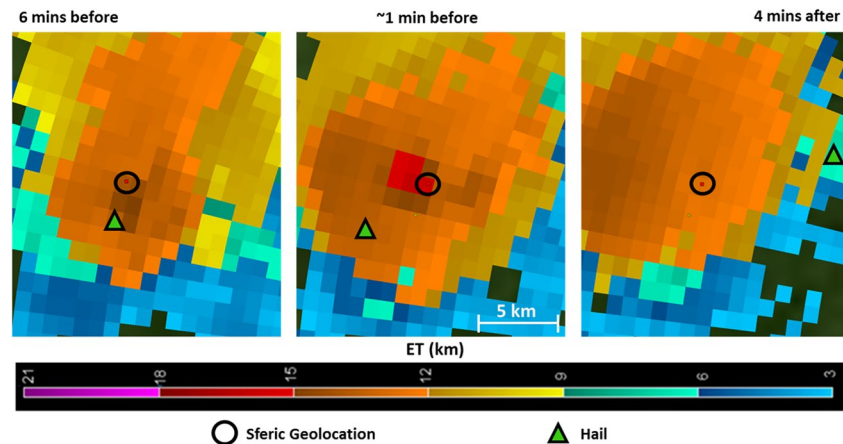
VILD of 0.46 g/m^3 for the lowest altitude event (Table 7). It should be noted that hail is rare in Baton Rouge: Stormersite reports a total of six reports of hail at ground level in the Baton Rouge area during 2015–2018. Amburn and Wolf (1997), however, cite a level of 1.6 g/m^3 as a VILD level appropriate for identifying events with hail with >0.75 in diameter. The presence in Table 7 of six of nine events with VILD > 1.6 g/m^3 is an indication of strong updrafts and high turbulent activity.

Chronis et al. (2016) have reported a lower bound for maximum VILD associated with Fermi TGFs of 0.54 g/m^3, compared to the lower bound maximum value of 0.46 g/m^3 seen in Table 7. Max values have a large range: 0.46–3.75, where the lowest is related to the relatively weak cold weather storm 190315 (with no hail and low lightning frequency) and the highest is related to 170325a in a squall-line storm with >1 in hail and high lightning frequency. The wide range of VILD values for TGFs observed by Chronis et al. (2016) is similar to the variation seen in the ground-level TETRA-II events.

Figure 5 shows box and whisker plots for ET (Figure 5a, top) and VILD (Figure 5b, bottom) for the TETRA-II events in the NEXRAD monitoring region. For each event, the range of ET and VILD are shown for the radar scan corresponding most closely to the X-ray/gamma-ray event, and also for the scans immediately preceding and immediately following the TETRA-II event (with an average of 7.6 min between the scan before the event and the scan after the event).

Almost all TETRA-II X-ray/gamma-ray flashes occur within minutes (before or after) of the peak ET and/ or VILD (Figure 5) or near in time to a lightning jump (Figure 3). Events 160427, 160919, and 170307 show a statistically significant drop in both VILD and ET minutes after the X-ray/gamma-ray event occurs. These events also occur near lightning jumps within the storms. The X-ray/gamma-ray flashes occurring on 170325 were broken into two groups depending on the time of the flash and the available scans. The first (170325a) shows an ET drop minutes after the TETRA-II event. The VILD median value increases (although the maximum value drops), indicating a sustained storm cell remained after the X-ray/gamma-ray event. VILD also drops significantly after 170325bc. The next three storms associated with TETRA-II events 170624abc, 180815, and 180817 were multicell storms in which the range of measured VILD values lowered significantly after the event. They also occurred near hail cells and lightning jumps within the 3 km radius. After the three X-ray/gamma-ray events on 170624, the VILD values dropped significantly, but the ET values rose, indicating a maximum updraft was reached post event. The VILD, however, indicates maximum ice

Figure 6. Echo tops of thunderstorm-producing event 160919 before, during, and after observed time of TETRA-II event. Image is centered on TETRA-II sensor location.

content decreased, indicating the collision and electrification potential within the system also decreased. Several lightning jumps also occurred after this event. ETs dropped significantly and lightning activity decreased after the event on 180815. On 180817, VILD peaks before the scan nearest to the event, indicating a sustained cell. No >2σ lightning jump occurs in the immediate vicinity of the X-ray/gamma-ray event, but hail was produced by the system after the gamma-ray event, and this may be related to the electrification of the ambient field. The final X-ray/gamma-ray flash on 190315 shows a drop in ET and VILD after the event. Eight of the nine events showed statistically significant decreases in either ET or VILD values post the gamma flash event indicating the event occurred near a peak in the system as represented by ET and VILD.

Figure 6 shows a sequence of ET scans of event 160919 beginning 6 min before, <1 min before, and 4 min after the event, demonstrating again that the TETRA-II event occurred close to the time of peak ET near TETRA-II. Images from radar scans for the eight other storms with NEXRAD coverage are shown in the Supplemental Material, indicating that the TETRA-II events occur consistently at or near peak height, that is, near maximum development of the updrafts and presumably also particle mixing, regardless of absolute storm height. This is evident, in particular, during the severe thunderstorm events (160919, 170325abc, and 170624abc), when ET peak duration lasted 3–20 min encompassing the time of the gamma-ray emission.

Figure 7 shows a sequence of VILD scans of event 180815 observed 9 min before, 3 min before, and 3 min after the event. The TETRA-II X-ray/gamma-ray event occurred close to the time of peak VILD and near the hail cell observed northwest of the event. Images of sequential radar scans for ET and VILD for all the Utuado and Baton Rouge events are shown in the Supplemental Material. All TETRA-II events in the NEXRAD coverage region occur nearby maximum VILD or ET, again indicating that the events occur at or near maximum development of the updrafts and presumably also particle mixing, regardless of absolute storm height.

These results based on ET and VILD values are derived from radar scans taken typically 5 min apart. This may be why the positions of the lightning and the hail cells do not match perfectly in Figures 6 and 7. H. Zhang et al. (2020) have compared Fermi GBM data with low frequency sferic data for a sample of equatorial TGFs observed from space, and found that the lightning occurs in the strong but not necessarily the strongest convection region of the storm. Although the TETRA-II results clearly indicate that the X-ray/gamma-ray events occur at or near maximum updraft development, the limited time resolution of the ground-based radar data is insufficient to distinguish between the actual peak of the storm versus the period just below peak activity.
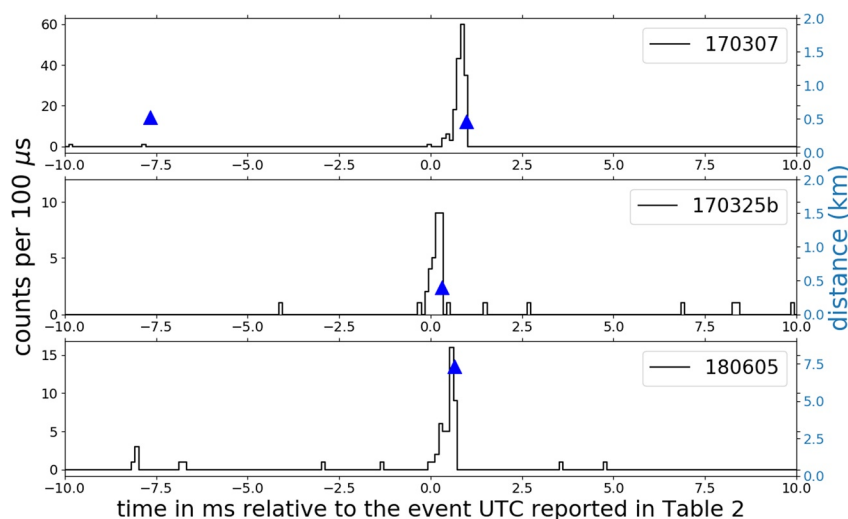
3.4. Anomalous Event 170707

Of the 22 initial TETRA-II events, 20 were accompanied by a nearby lightning strike at distances ranging from 0.2 to 6.8 km, with the associated sferic occurring between 10 μs and 1.3 ms after the beginning of the X-ray/gamma-ray event and typically within ~100 μs of the end of the gamma-ray event, supporting
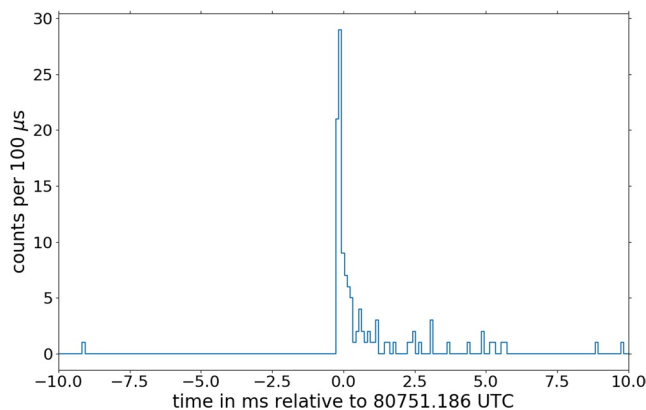
Figure 7. VILD of thunderstorm producing event 180815 before, during, and after observed time of TETRA-II event. Images are centered on the sferic, 0.5 km from TETRA II.

the argument that these events were produced during the later stages of the lightning step leader process (Pleshinger et al., 2019). As discussed in Section 1, the majority of the events had a characteristic stepped time profile, rising in intensity until an abrupt cutoff near the time of the sferic (Figure 8). Most of the remaining events had a relatively symmetrical time structure. The single exception was event 170707 observed in Baton Rouge, in which the signal rose abruptly and then decayed away over ~5 ms (Figure 9).

Event 170707 occurred in conjunction with a severe deep-convection quasi-stationary thunderstorm exhibiting lightning activity, with its core 15 km east of TETRA-II (Figure 10). No lightning strokes were observed within 8 km and 3 s of the X-ray/gamma-ray flash, suggesting that 170707 was not associated with a nearby leader. The rapid rise and slower decline in the count rate suggests a similarity to the neutron-induced events seen in Japan (Bowers et al., 2017; Enoto et al., 2017), but the Japanese neutron events are significantly longer (tens of ms to seconds). 170707 also has similarities to cosmic ray events in Fermi GBM (Figure S9 in the supporting information).

Figure 8. Time profiles of TETRA-II events 170307, 170325b, and 180605. Left-hand scale shows the number of gamma-rays detected per 100 μs over a 20 ms time span around the event. Blue triangles mark the times of nearby sferics, with the distance to the sferic shown on the right-hand scale.
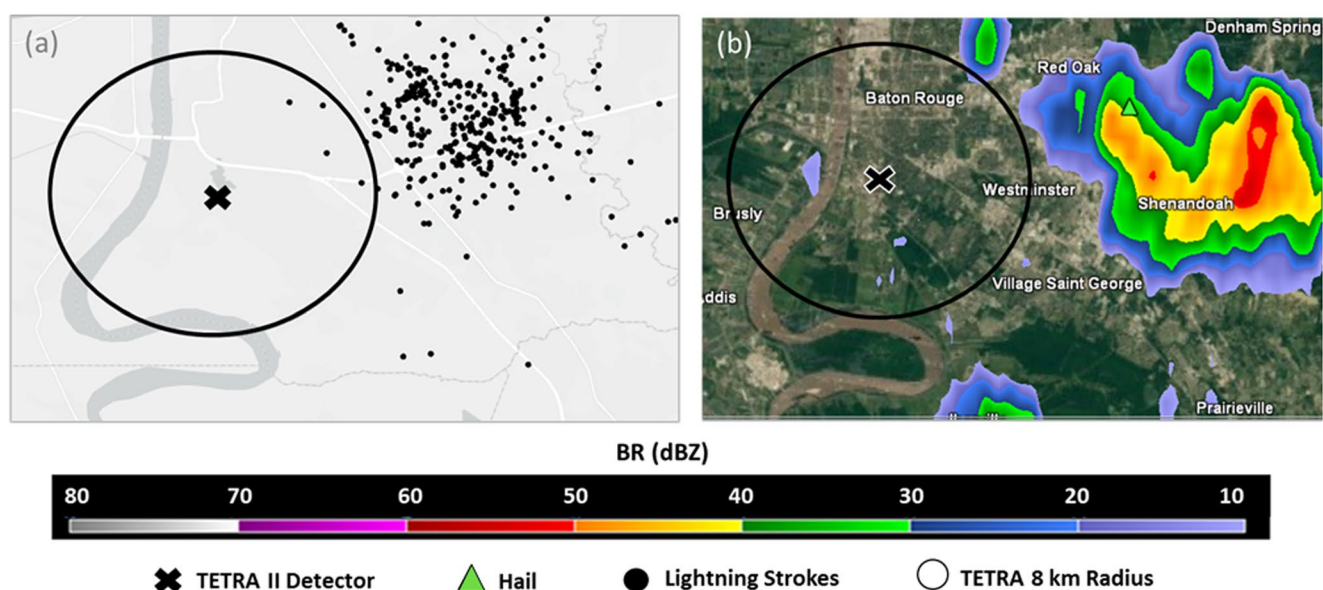
Figure 9. Event 170707, showing gamma-rays detected per 100 μs over a 20 ms time span around the event.

4. Conclusions

Properties of thunderstorms associated with bright X-ray/gamma-ray bursts detected at ground-level by the TETRA-II arrays have been analyzed. Lightning stroke characteristics have been used to infer properties of the electric field and phase of updraft development, and NEXRAD radar scans have been used to characterize thunderstorm structure and quantify convective features. Average lightning stroke rates within event-producing thunderstorms range from sparse (<1/min) to dense (46/min) in the mature phase of development, demonstrating that the X-ray/gamma-ray flash can be produced in thunderstorms with varying electrical activity. The majority of events occurred within 5 min of a lightning jump/peak, and in the case of low stroke rate storms, within seconds (and sometimes milliseconds) of peak lightning. These results indicate a connection between X-ray/gamma-ray occurrence and the intensification of the updraft and cloud electrification regardless of average stroke rate.

Events within the NEXRAD-monitoring region (Baton Rouge and Utuado) were produced in thunderstorms ranging from moderate convective multicell to severe squall line thunderstorms with cells of large horizontal extent (>40 km^2). Events were not observed during single-cell thunderstorms. Events occur within thunderstorm cells with updrafts persisting to mixed-phase cloud altitudes characterized by estimated maximum thunderstorm heights ranging between 8.8 and 16.3 km. Though events occur in a range of thunderstorms, they tend to occur in conjunction with updraft intensification marked by ETs at or nearing peak altitude and/or peak VILD values. Maximum values of VILD in TETRA II thunderstorms have a relatively large range (0.46–3.75 g/m^3) also indicating a wide variety of thunderstorms capable of producing TETRA II gamma-ray events. Additionally, all but one event within the NEXRAD monitoring region occur in the presence of detectable hail cells.

TETRA II event characteristics and thunderstorm altitudes are generally consistent with reports of Fermi, AGILE, and RHESSI TGF events (Chronis et al., 2016; Ursi et al., 2019) with the exception of one cold-weather, low-stroke event (190315). Chronis et al. (2016) suggested that a lack of lower altitude TGFs detected by Fermi and RHESSI is due to the increased attenuation that photons from lower altitudes are

Figure 10. Event 170707 in Baton Rouge. (a) Location of lightning detected near TETRA II in Baton Rouge within 10 min of event 170707. Circle shows 8 km radius around TETRA-II location. Only four lightning strokes were detected within 8 km and 10 min of the gamma-ray event, none within 3 s of the event. (b) BR scan at time of the gamma-rays, showing the main storm activity well to the east of the TETRA-II detector site.

subject to before reaching the satellite sensors. The detection of the TETRA-II event 190315 with estimated cloud top altitude of 8.8 km substantiates this assertion, as this low thunderstorm height is significantly lower than the events detected from space (Chronis et al., 2016; Smith et al., 2010; Splitt et al., 2010). This event is also associated with the lowest value of maximum VILD (0.46 g/m^3) which is similar to the lowest bound of VILD values for Fermi TGFs (0.54 g/m^3). These results further indicate that absolute high altitude convection and storm severity is not a requirement for TETRA-II X-ray/gamma-ray events.

TETRA-II events demonstrate that varying thunderstorm structures and convective strengths have properties suitable for the production of ground-beamed X-ray/gamma-ray events, and that the events observed at ground level by TETRA-II are preferentially associated with the maximum intensification of the thunderstorms. The distribution of ETs and VILD is relatively large in range, suggesting that thunderstorms of varying convective characteristics are capable of producing similar gamma-ray events and again that there is a strong connection between X-ray/gamma-ray production and thunderstorm updraft strength and intensification. The association with maximum thunderstorm development and electrification is measured by lightning jumps, the presence of hail cells, and the peaks in measured ET and VILD regardless of absolute height. TETRA-II continues operation in order to accumulate additional events and improved statistics.

Data Availability Statement

Lightning data were provided by Vaisala-GLD360 (https://www.vaisala.com/en/products/data-subscriptions-and-reports/data-sets/gld360), Vaisala-NLDN (https://www.vaisala.com/en/products/data-subscriptions-and-reports-/datasets-/nldn): and WWLLN (http://wwlln.net/). Weather and radar data were provided by NEXRAD (https://www.ncdc.noaa.gov/nexradinv/), NWS (https://www.weather.gov/bgm/severedefinitions), and StormerSite (https://www.stormersite.com/hail-history-reports). TETRA-II data are available online at https://tetra.phys.lsu.edu.

References

Abarca, S., Corbosiero, K., & Galarneau, T., Jr. (2010). An evaluation of the Worldwide Lightning Location Network (WWLLN) using the National Lightning Detection Network (NLDN) as ground truth. *Journal of Geophysical Research*, *115*, D18206. https://doi.org/10.1029/2009jd013411

Abbasi, R., Abe, M., Abu-Zayyad, T., Allen, M., Anderson, R., Azuma, R., et al. (2017). The bursts of high energy events observed by the Telescope Array surface detector. *Physics Letters A*, *381*(32), 2565–2572

Aggarwal, G., Mishra, N., & Pinkas, B. (2010). Secure computation of the median (and other elements of specified ranks). *Journal of Cryptology*, *23*(3), 373–401. https://doi.org/10.1007/s00145-010-9059-9

Albrecht, R., Goodman, S., Buechler, D., Blakeslee, R., & Christian, H. (2016). Where are the lightning hotspots on earth? *Bulletin of the American Meteorological Society*, *97*(11), 2051–2068.

Albrechtsen, K., Ostgaard, N., Berge, N., & Gjesteland, T. (2019). Observationally weak TGFS in the RHESSI data. *Journal of Geophysical Research: Atmospheres*, *124*(1), 287–298. https://doi.org/10.1029/2018jd029272

Amburn, S. A., & Wolf, P. L. (1997). VIL density as a hail indicator. *Weather and Forecasting*, *12*(3), 473–478. https://doi.org/10.1175/1520-0434(1997)012<0473:vdaahi>2.0.co;2

Babich, L., Bochkov, E., Kutsyk, I., Neubert, T., & Chanrion, O. (2015). A model for electric field enhancement in lightning leader tips to levels allowing X-ray and gamma ray emissions. *Journal of Geophysical Research: Space Physics*, *120*(6), 5087–5100. https://doi.org/10.1002/2014ja020923

Barnes, D. E., Splitt, M. E., Dwyer, J. R., Lazarus, S., Smith, D., & Rassoul, K. (2015). A study of thunderstorm microphysical properties and lightning flash counts associated with Terrestrial Gamma-ray Flashes. *Journal of Geophysical Research: Atmospheres*, *120*, 3453–3464. https://doi.org/10.1002/2014jd021495

Belz, J. W., Krehbiel, P. R., Remington, J., Stanley, M., Abbasi, R. U., LeVon, R., & Zundel, Z. (2020). Observations of the origin of downward Terrestrial Gamma-ray Flashes. *Journal of Geophysical Research: Atmospheres*, *125*, e2019JD031940. https://doi.org/10.1029/2019JD031940

Bowers, G., Smith, D., Kelley, N., Martinez-McKinney, G., Cummer, S., Dwyer, J., et al. (2018). A Terrestrial Gamma-ray Flash inside the Eyewall of Hurricane Patricia. *Journal of Geophysical Research: Atmospheres*, *123*(10), 4977–4987. https://doi.org/10.1029/2017jd027771

Bowers, G., Smith, D., Martinez-McKinney, G., Kamogaw, M., Cummer, S., Dwyer, J., & Kawasaki, Z. (2017). Gamma ray signatures of neutrons from a Terrestrial Gamma-ray Flash. *Geophysical Research Letters*, *44*(10), 063–070. https://doi.org/10.1002/2017gl075071

Briggs, M., Fishman, G., Connaughton, V., Bhat, P., Paciesas, W., Preece, R., & Von Kienlin, A. (2010). First results on terrestrial gamma-ray flashes from the Fermi Gamma-ray Burst Monitor. *Journal of Geophysical Research*, *115*(A7), A07323. https://doi.org/10.1029/2009ja015242

Carlson, B., Lehtinen, N., & Inan, U. (2010). Terrestrial gamma-ray flash production by active lightning leader channels. *Journal of Geophysical Research*, *115*(A10), A015647. https://doi.org/10.1029/2010ja015647

Celestin, S., & Pasko, V. P. (2011). Energy and fluxes of thermal runaway electrons produced by exponential growth of streamers during the stepping of lightning leaders and in transient luminous events. *Journal of Geophysical Research*, *116*(A3), 1–7. https://doi.org/10.1029/2010ja016260

Changnon, S. A. (1992). Temporal and spatial relations between hail and lightning. *Journal of Applied Meteorology*, *31*(6), 587–604. https://doi.org/10.1175/1520-0450(1992)031<0587:tasrbh>2.0.co;2

Chilingarian, A., Daryan, A., Arakelyan, K., Hovhannisyan, A., Mailyan, B., Melkumyan, L., & Vanyan, L. (2010). Ground-based observations of thunderstorm-correlated fluxes of high-energy electrons, Gamma-rays, and neutrons. *Physical Review D*, *82*(4), 043009. https://doi.org/10.1103/physrevd.82.043009

Chronis, T., Briggs, M., Priftis, G., Connaughton, V., Brundell, J., Holzworth, R., et al. (2016). Characteristics of Thunderstorms that Produce Terrestrial Gamma-ray Flashes. *Bulletin of the American Meteorological Society*, *97*, 639–653. https://doi.org/10.1175/bams-d-14-00239.1

Connaughton, V., Briggs, M., Holzworth, R., Hutchins, M., Fishman, G., Wilson-Hodge, C., & Von Kienlin, A. (2010). Associations between Fermi Gamma-ray Burst Monitor terrestrial gamma-ray flashes and sferics from the world wide lightning location network. *Journal of Geophysical Research*, *115*(A12), A015681. https://doi.org/10.1029/2010ja015681

Connaughton, V., Briggs, M., Xiong, S., Dwyer, J., Hutchins, M., Grove, J., et al. (2013). Radio signals from electron beams in Terrestrial Gamma-ray Flashes. *Journal of Geophysical Research: Space Physics*, *118*, A018218. https://doi.org/10.1029/2012ja018288

Cummer, S., Briggs, M., Dwyer, J., Xiong, S., Connaughton, V., Fishman, G., et al. (2014). The source altitude, electric current, and intrinsic brightness of terrestrial gamma flashes. *Geophysical Research Letters*, *41*, 8586–8593. https://doi.org/10.1002/2014gl062196

Cummer, S., Lyu, F., Briggs, M., Fitzpatrick, G., Roberts, O., & Dwyer, J. (2015). Lightning leader altitude progression in terrestrial gamma-ray flashes. *Geophysical Research Letters*, *42*, 7792–7798. https://doi.org/10.1002/2015gl065228

Cummins, K., Krider, E., & Malone, M. (1998). The U.S. National Lightning Detection Network™ and applications of cloud-to-ground lightning data by electric power utilities. *IEEE Transactions on Electromagnetic Compatibility*, *40*, 465–480. https://doi.org/10.1109/15.736207

Cummins, K., Murphy, M., Bardo, E., Hiscox, W., Pyle, R., & Pifer, A. (1998). A combined TOA/MDF technology upgrade of the US National Lightning Detection Network. *Journal of Geophysical Research*, *103*(D8), 9035–9044. https://doi.org/10.1029/98jd00153

Dahl, J. M. L., Höller, H., & Schumann, U. (2011). Modeling the flash rate of thunderstorms. Part I: Framework. *Monthly Weather Review*, *139*(10), 3093–3111. https://doi.org/10.1175/mwr-d-10-05031.1

Dash, J., & Wettlaufer, J. (2003). The surface physics of ice in thunderstorms. *Canadian Journal of Physics*, *81*(1–2), 201–207. https://doi.org/10.1139/p03-011

Dwyer, J. (2012). The relativistic feedback discharge model of terrestrial gamma ray flashes. *Journal of Geophysical Research*, *117*(A02308), 1–25. https://doi.org/10.1029/2011ja017160

Dwyer, J., Grefenstette, B. W., & Smith, D. M. (2008). High-energy electron beams launched into space by thunderstorms. *Geophysical Research Letters*, *35*(2), L02815. https://doi.org/10.1029/2007gl032430

Dwyer, J., Rassoul, H., Al-Dayeh, M., Caraway, L., Wright, B., Chrest, A., et al. (2004). A ground level gamma-ray burst observed in association with rocket-triggered lightning. *Geophysical Research Letters*, *31*(5), L05119. https://doi.org/10.1029/2003gl018771

Dwyer, J., Rassoul, H. K., Al-Dayeh, M., Caraway, L., Chrest, A., Wright, B., et al. (2005). X-ray bursts associated with leader steps in cloud-to-ground lightning. *Geophysical Research Letters*, *32*(1), L01803. https://doi.org/10.1029/2004gl021782

Dwyer, J., & Smith, D. (2005). A comparison between Monte Carlo simulations of runaway breakdown and terrestrial gamma-RAY flash observations. *Geophysical Research Letters*, *32*(22), L22804. https://doi.org/10.1029/2005gl023848

Emersic, C., & Saunders, C. (2010). Further laboratory investigations into the relative diffusional growth rate theory of thunderstorm electrification. *Atmospheric Research*, *98*(2–4), 327–340. https://doi.org/10.1016/j.atmosres.2010.07.011

Enoto, T., Wada, Y., Furuta, Y., Nakazawa, K., Yuasa, T., Okuda, K., et al. (2017). Photonuclear reactions triggered by lightning discharge. *Nature*, *551*(7681), 481–484. https://doi.org/10.1038/nature24630

Fabró, F., Montanyà, J., Marisaldi, M., van der Velde, O. A., & Fuschino, F. (2015). Analysis of global terrestrial gamma-ray flashes distribution and special focus on AGILE detections over South America. *Journal of Atmospheric and Solar-Terrestrial Physics*, *124*, 10–20. https://doi.org/10.1016/j.jastp.2015.01.009

Fishman, G., Bhat, P., Mallozzi, R., Horack, J., Koshut, T., Kouveliotou, C., et al. (1994). Discovery of intense Gamma-ray Flashes of atmospheric origin. *Science*, *264*(5163), 1313–1316. https://doi.org/10.1126/science.264.5163.1313

Gatlin, P. N., & Goodman, S. J. (2010). A total lightning trending algorithm to identify severe thunderstorms. *Journal of Atmospheric and Oceanic Technology*, *27*(1), 3–22. https://doi.org/10.1175/2009jtecha1286.1

Grefenstette, B., Smith, D., Hazelton, B., & Lopez, L. (2009). First RHESSI Terrestrial Gamma-ray Flash catalog. *Journal of Geophysical Research*, *114*(A2), A02314. https://doi.org/10.1029/2008ja013721

Gurevich, A., Milikh, G., & Roussel-Dupre, R. (1992). Runaway electron mechanism of air breakdown and preconditioning during a thunderstorm. *Physics Letters A*, *165*(5–6), 463–468. https://doi.org/10.1016/0375-9601(92)90348-p

Hare, B., Uman, M., Dwyer, J., Jordan, D., Biggerstaff, M., Caicedo, J., et al. (2016). Ground-level observation of a terrestrial gamma-ray flash initiated by a triggered lightning. *Journal of Geophysical Research: Atmospheres*, *121*(11), 6511–6533. https://doi.org/10.1002/2015jd024426

Houze, R. A. (2014). *Cloud dynamics* (Vol. 104). Academic Press.

Hutchins, M., Holzworth, R., Brundell, J., & Rodger, C. (2012). Relative detection efficiency of the World Wide Lightning Location Network. *Radio Science*, *47*(06), 1–9. https://doi.org/10.1029/2012rs005049

Lindanger, A., Marisaldi, M., Maiorana, C., Sarria, D., Albrechtsen, K., et al. (2020). The 3rd AGILE terrestrial gamma-ray flash catalog. Part I: Association to lightning sferics. *Journal of Geophysical Research: Atmospheres*, *125*, e2019JD031985. https://doi.org/10.1029/2019jd031985

Lu, G., Blakeslee, R. J., Li, J., Smith, D. M., Shao, X.-M., McCaul, E. W., & Cummer, S. A. (2010). Lightning mapping observation of a terrestrial gamma-ray flash. *Geophysical Research Letters*, *37*(11), L11806. https://doi.org/10.1029/2010gl043494

Lu, G., Cummer, S. A., Li, J., Han, F., Smith, D. M., & Grefenstette, B. W. (2011). Characteristics of broadband lightning emissions associated with terrestrial gamma-ray flashes. *Journal of Geophysical Research*, *116*(A3), A03316. https://doi.org/10.1029/2010ja016141

MacGorman, D. R., & Morgenstern, C. D. (1998). Some characteristics of cloud-to-ground lightning in mesoscale convective systems. *Journal of Geophysical Research*, *103*(D12), 14011–14023. https://doi.org/10.1029/97jd03221

Mailyan, B. G., Nag, A., Dwyer, J., Said, R. K., Briggs, M. S., Roberts, O. J., et al. (2020). Gamma-ray and radio-frequency radiation from thunderstorms observed from space and ground. *Scientific Reports*, *10*, 7286. https://doi.org/10.1038/s41598-020-63437-2

Mailyan, B. G., Nag, A., Murphy, M. J., Briggs, M., Dwyer, J., Riso, W., et al. (2018). Characteristics of radio emissions associated with terrestrial gamma-ray flashes. *Journal of Geophysical Research: Space Physics*, *123*, 5933–5948. https://doi.org/10.1029/2018ja025450

Maiorana, C., Marisaldi, M., Lindanger, A., Østgaard, N., Ursi, A., Sarria1, D., & Verrecchia, F. (2020). The 3rd AGILE terrestrial gamma-ray flashes catalog. Part II: Optimized selection criteria and characteristics of the new sample. *Journal of Geophysical Research: Atmospheres*, *125*, e2019JD031986. https://doi.org/10.1029/2019jd031986

Mallick, S., Rakov, V., & Dwyer, J. R. (2012). A study of X-ray emissions from thunderstorms with emphasis on subsequent strokes in natural lightning. *Journal of Geophysical Research*, *117*(D16), D16107. https://doi.org/10.1029/2012jd017555

Marisaldi, M., Arga, A., Urs, A., Gjestelan, T., Fuschin, F., Labanti, C, et al. (2015). Enhanced detection of terrestrial gamma-ray flashes by AGILE. *Geophysical Research Letters*, *42*, 9481–9487. https://doi.org/10.1002/2015gl066100

Marisaldi, M., Fuschino, F., Labanti, C., Galli, M., Longo, F., Del Monte, E., & Moretti, E. (2010). Detection of terrestrial gamma-ray flashes up to 40 MeV by the AGILE satellite. *Journal of Geophysical Research*, *115*(A3), A00E13. https://doi.org/10.1029/2009JA014502

Merceret, F. J., Ward, J. G., Mach, D. M., Bateman, M. G., & Dye, J. E. (2008). On the magnitude of the electric field near thunderstorm-associated clouds. *Journal of Applied Meteorology and Climatology*, *47*(1), 240–248. https://doi.org/10.1175/2007jamc1713.1

Miller, P., Ellis, A. W., & Keighton, S. (2015). A preliminary assessment of using spatiotemporal lightning patterns for a binary classification of thunderstorm mode. *Weather and Forecasting*, *30*(1), 38–56. https://doi.org/10.1175/waf-d-14-00024.1

Moore, C., Eack, K., Aulich, G., & Rison, W. (2001). Energetic radiation associated with lightning stepped-leaders. *Geophysical Research Letters*, *28*, 2141–2144. https://doi.org/10.1029/2001gl013140

National Weather Service (2019). *Severe Weather Definitions*. United States. https://www.weather.gov/bgm/severedefinitions

Østgaard, N., Albrechtsen, K., Gjesteland, T., & Collie, A. (2015). A new population of terrestrial gamma-ray flashes in the RHESSI data. *Geophysical Research Letters*, *42*, 10937. https://doi.org/10.1002/2015gl067064

Østgaard, N., Neubert, T., Reglero, V., Ullaland, K., Yang, S., Genov, G., et al. (2019). First 10 months of TGF observations by ASIM. *Journal of Geophysical Research: Atmospheres*, *124*(24), 14024–14036. https://doi.org/10.1029/2019jd031214

Panasyuk, M., Svertilov, S., Bogomolov, V., Garipov, G., Balan, E., Barinova, V., et al. (2016). RELEC mission: Relativistic electron precipitation and TLE study on-board small spacecraft. *Advances in Space Research*, *57*(3), 835–849. https://doi.org/10.1016/j.asr.2015.11.033

Pleshinger, D. J., Alnussirat, S. T., Bai, S., Banadaki, Y., Cherry, M. L., Hoffman, J. H., et al. (2019). Gamma-ray flashes produced by lightning observed at ground level by TETRA-II. *Journal of Geophysical Research: Space Physics*, *124*(11), 9229–9238. https://doi.org/10.1029/2019ja026820

Pruppacher, H. R., & Klett, J. D. (2010). Microphysics of clouds and precipitation. In Pruppacher, H. R., & Klett, J. D. (Eds.), *Microstructure of atmospheric clouds and precipitation* (pp. 10–73). Springer. https://doi.org/10.1007/978-0-306-48100-0_2

Ringuette, R., Case, G. L., Cherry, M. L., Granger, D., Guzik, T. G., Stewart, M., & Wefel, J. P. (2013). TETRA observation of gamma-rays at ground level associated with nearby thunderstorms. *Journal of Geophysical Research: Space Physics*, *118*(12), 7841–7849. https://doi.org/10.1002/2013ja019112

Roberts, O., Fitzpatrick, G., Stanbro, M., McBreen, S., Briggs, M., Holzworth, R., et al. (2018). The FirstFermi-GBM Terrestrial Gamma-ray Flash Catalog. *Journal of Geophysical Research: Space Physics*, *123*(5), 4381–4401. https://doi.org/10.1029/2017ja024837

Rudlosky, S., Peterson, M., & Kahn, D. (2017). GLD360 performance relative to TRMM LIS. *Journal of Atmospheric and Oceanic Technology*, *34*, 1307–1322. https://doi.org/10.1175/jtech-d-16-0243.1

Rudlosky, S., & Shea, D. (2013). Evaluating WWLLN performance relative to TRMM/LIS. *Geophysical Research Letters*, *40*, 2344–2348. https://doi.org/10.1002/grl.50428

Said, R., & Murphy, M. (2016). GLD360 upgrade: Performance analysis and applications. In *Proceedings of 24th international lightning detection conference & 6th international lightning meteorology conference*. (pp. 18–21). San Diego, CA. Retrieved from https://www.vaisala.com/sites/default/files/documents/Ryan%20Said%20and%20Martin%20Murphy.%20GLD360%20Upgrade%20Performance%20Analysis%20and%20Applications.pdf

Saleh, Z., Dwyer, J., Howar, J., Uman, M., Bakhtiar, M., Concha, D., & Rassoul, H. (2020). Properties of the X-ray emission from rocket-triggered lightning as measured by the Thunderstorm Energetic Radiation Array (TERA). *Journal of Geophysical Research: Atmospheres*, *114*(5), D17210. https://doi.org/10.1029/2008JD011618

Saunders, C. (2008). Charge separation mechanisms in clouds. *Space Science Reviews*, *137*(1–4), 335–353. https://doi.org/10.1007/978-0-387-87664-1_22

Schultz, C. J., Carey, L. D., Schultz, E. V., & Blakeslee, R. J. (2015). Insight into the kinematic and microphysical processes that control lightning jumps. *Weather and Forecasting*, *30*(6), 1591–1621. https://doi.org/10.1175/waf-d-14-00147.1

Shao, X.-M., Hamlin, T., & Smith, D. M. (2010). A closer examination of terrestrial gamma-ray flash-related lightning processes. *Journal of Geophysical Research*, *115*(A6), A00E30. https://doi.org/10.1029/2009ja014835

Smith, D., Buzbe, P., Kelle, N., Infang, A., Holzworth, R., & Dwyer, J. (2016). The rarity of terrestrial gamma-ray flashes: 2. RHESSI stacking analysis. *Journal of Geophysical Research: Atmospheres*, *121*, 11382. https://doi.org/10.1002/2016jd025395

Smith, D., Dwyer, J., Hazelton, B., Grefenstette, B., Martinez-McKinney, G., Zhang, Z., et al. (2011). A terrestrial gamma-ray flash observed from an aircraft. *Journal of Geophysical Research*, *116*(D20), D20124. https://doi.org/10.1029/2011jd016252

Smith, D., Hazelton, B., Grefenstette, B., Dwyer, J., Holzworth, R., & Lay, E. (2010). Terrestrial Gamma-ray Flashes correlated to storm phase and tropopause height. *Journal of Geophysical Research*, *115*(A8), A00E49. https://doi.org/10.1029/2009ja014853

Splitt, M. E., Lazarus, S. M., Barnes, D., Dwyer, J. R., Rassoul, H. K., Smith, D. M., & Grefenstette, B. W. (2010). Thunderstorm characteristics associated with RHESSI-identified terrestrial gamma-ray flashes. *Journal of Geophysical Research*, *115*, A00138. https://doi.org/10.1029/2009ja014622

Stanley, M. A., Shao, X.-M., Smith, D. M., Lopez, L. I., Pongratz, M. B., Harlin, J. D., et al. (2006). A link between terrestrial gamma-ray flashes and intracloud lightning discharges. *Geophysical Research Letters*, *33*(6), L06803. https://doi.org/10.1029/2005gl025537

Tran, M., Rakov, V., Mallick, S., Dwyer, J., Nag, A., & Heckman, S. (2015). A terrestrial gamma-ray flash recorded at the Lightning Observatory in Gainesville, Florida. *Journal of Atmospheric and Solar-Terrestrial Physics*, *136*, 86–93. https://doi.org/10.1016/j.jastp.2015.10.010

Ursi, A., Guidorzi, C., Marisaldi, M., Sarria, D., & Frontera, F. (2017). Terrestrial gamma-ray flashes in the BeppoSAX data archive. *Journal of Atmospheric and Solar-Terrestrial Physics*, *156*, 50–56. https://doi.org/10.1016/j.jastp.2017.02.014

Ursi, A., Marisald, M., Dietric, S., Tavani, M., Tiberia, A., & Porcù, F. (2019). Analysis of thunderstorms producing terrestrial gamma-ray flashes with the Meteosat Second Generation. *Journal of Geophysical Research: Atmospheres*, *124*, 12667–12682. https://doi.org/10.1029/2018jd030149

Wada, Y., Enoto, T., Nakamura, Y., Furuta, Y., Yuasa, T., Nakazawa, K., et al. (2019). Gamma-ray glow preceding downward terrestrial gamma-ray flash. *Communications on Physics*, *2*, 67. https://doi.org/10.1038/s42005-019-0168-y

Wada, Y., Enoto, T., Nakazawa, K., Furuta, Y., Yuasa, T., Nakamura, Y., & Tsuchiya, H. (2019). Downward terrestrial gamma-ray flash observed in a winter thunderstorm. *Physical Review Letters*, *123*, 061103. https://doi.org/10.1103/physrevlett.123.061103

Williams, E., Boldi, B., Matlin, A., Weber, M., Hodanish, S., Sharp, D., & Buechler, D. (1999). The behavior of total lightning activity in severe Florida thunderstorms. *Atmospheric Research*, *51*(3–4), 245–265. https://doi.org/10.1016/s0169-8095(99)00011-3

Williams, E., Boldi, R., Bor, J., Satori, G., Price, C., Greenberg, E., et al. (2006). Lightning flashes conducive to the production and escape of gamma radiation to space. *Journal of Geophysical Research*, *111*(D16), D16209. https://doi.org/10.1029/2005jd006447

Witt, A., Eilts, M. D., Stumpf, G. J., Johnson, J., Mitchell, E. D. W., & Thomas, K. W. (1998). An enhanced hail detection algorithm for the WS-88D. *Weather and Forecasting*, *13*(2), 286–303. https://doi.org/10.1175/1520-0434(1998)013<0286:aehdaf>2.0.co;2

Xu, W., Celestin, S., & Pasko, V. P. (2012). Source altitudes of terrestrial gamma-ray flashes produced by lightning leaders. *Geophysical Research Letters*, *39*(8), L08801. https://doi.org/10.1029/2012gl051351

Zhang, D., Cummins, K., Nag, A., Murphy, M., & Bitzer, P. (2016). Evaluation of the national lightning detection network upgrade using the lightning imaging sensor. In *Proceedings of 24th International Lightning detection Conference & 6th International Lightning Meteorology Conference*. (pp. 18–21). San Diego, CA.

Zhang, H., Lu, G., Lyu, F., Ahma, M., Qie, X., Cummer, S., & Briggs, M. (2020). First measurements of low-frequency sferics associated with terrestrial gamma-ray flashes produced by equatorial thunderstorms. *Geophysical Research Letters*, *47*, e2020GL089005. https://doi.org/10.1029/2020gl089005